

PROPAGATION CHARACTERISTICS OF THE SPACE CHANNEL

ELIE J. BAGH DADY
ADCOM. Inc.
Cambridge, Massachusetts

Abstract A discussion is provided of the propagation phenomena, and their associated disturbances, that have been observed to cause significant degradation of the performance of space instrumentation and communication links.

1.0 Introduction An adequate characterization of the space transmission medium is an essential requirement in the design of all space instrumentation and information transfer systems. The ultimate objective of such a characterization is to provide the system designer and analyst with a description of the transmission disturbances in terms of measurable or predictable parameters, so that a quantitative evaluation can be made of the degradation in information transfer and the measurement errors caused by adverse conditions between receiving and transmitting antennas. Unfortunately, our current understanding of several important phenomena affecting signal propagation to and from space vehicles is far from the level required for a reasonably close quantitative estimation of the necessary parameters.

The unavoidable transmission disturbances may be classified into additive and propagation disturbances. In this paper, we are principally concerned with the propagation disturbances. For this reason, the discussion of additive disturbances is restricted to a brief description to distinguish them from the propagation disturbances.

In the discussion of the propagation disturbances, attention is directed to space links with one terminal on the earth's surface. The transmission channel between the terminals is categorized on the basis of phases of a complete mission in which the geometry of transmission paths and composition of the intervening medium show distinctive characteristics. In some of these phases, the characteristics of the channel change quite rapidly, in others they remain fairly regular over extended time intervals. Emphasis in the present discussion is placed on the gross characteristics of multipath and plasmas. The discussion relating to plasmas is necessarily restricted to the results of gross experimental observations, inasmuch as the analysis of plasmas in all but the most academic and totally inapplicable cases continues to be completely intractable, and only recently has a drive for a systematic and comprehensive program of experimentation been organized.

2.0 Additive Disturbances Additive disturbances are those that are added to the desired signal from unwanted sources as original radiations that are (except for certain types of deliberate jamming) causally independent of the desired signal. With the exception of certain types of deliberate jamming, the presence or absence of an additive disturbance in the receiver passband is independent of the desired signal.

Additive disturbances may be subdivided into:

- a) Random-fluctuation noise, including receiver front-end. noise, earth-noise pickup by vehicle antenna and ground-antenna minor lobes, noise associated with all atmospheric absorption mechanisms, and galactic and inter-galactic noise. Solar, lunar and planetary noise are important when very narrow ground-antenna beams are used, but because their effect is momentary, they are not considered serious unless they can cause interruption of synchronized operation.
- b) CW-type interference from extraneous sources, including ground links in almost all frequency ranges, or from spurious products of front-end loading or mixing or from insufficient suppression of local RFI in the spacecraft, or in the ground station.
- c) Pulsed or impulsive disturbances mainly from othe requipment, such as radars.

This classification is based upon the fact that these three categories cause distinctly different interference effects, are most conveniently represented and analyzed by distinctly different analytical tools\$ and usually are best handled by peculiar suppression techniques.

The total effective random-fluctuation noise power at the receiver is usually expressed in terms of an operating thermal noise temperature. It is important to emphasize that although the operating thermal noise temperature of the receiving system is always an important system design consideration, the difficulties of maintaining performance reliability are often traceable to the presence of other signals or mixing by-products that disturb the receiver operations and corrupt the spectral region of the desired signal.

3.0 Propagation Disturbances Propagation disturbances are the effects upon the signal properties in time, introduced by the time -variant physical properties and geometry of the traversed medium. These effects may be perceived as modulation of the signal amplitude, of the phase (or frequency), of the polarization, and of the direction of arrival.

Propagation disturbances include variable attenuation due to absorption and scattering in the atmosphere (mainly the troposphere) and to geometrical divergence of power radiated. to or from a moving vehicle, optical distortions due to the intervening earth's

atmosphere and magnetic field, variable doppler due to relative motion, multipath caused by mainbeam and sidelobe pickup of reflected rays and by pressure shock waves in the atmosphere, and ionization and plasma attenuation and disturbances caused by rocket exhausts and by intense heating on exit or re-entry into the atmosphere.

Propagation through the earth's atmosphere subjects signals to refraction effects due to the variation of propagation phase velocity in the different layers of the earth's atmosphere. Irregular and randomly variant refraction results in two effects that are sometimes considered separately:

- a) a bending of the ray, amounting to a lengthening of the path of propagation, and
- b) a reduction in the group velocity resulting in an added extraneous time delay.

These propagation effects contribute significantly only to tracking errors. The total phase shifts are strongly dependent on the angle of elevation of the vehicle, because a smaller angle of elevation implies a longer distance to be traversed by the radio wave through the atmosphere. Phase shifts due to refraction can be appreciable but are quite stable in general. These phase shifts change slowly as the vehicle changes its elevation with respect to the ground station, and vary with diurnal changes in the propagation velocity in the various layers of the atmosphere. They are also dependent on the frequency of the radiated waves.

Ionospheric dispersion results from variations of the index of refraction of the ionized layers with frequency and may affect very wideband signals. This frequency dependence causes a variable time delay with frequency, which may not even be linear in the second-order effects, and may also be time -variant because it depends upon variable ionospheric conditions and upon the changing thickness of penetrated ionosphere.

For frequencies above 100 Mc, the most troublesome propagation effects and hence the ones of major interest in this paper - are those caused by plasmas and by multipath. Atmospheric refractive effects are of serious concern in precision tracking, but will not be emphasized here because of the considerable existing knowledge in that area and the progress under way in the methods for correcting or compensating for them.

4.0 Types of Space Channels Space channels are characterized by the great and rapid changes that can be expected in the geometry and the constitution of the medium linking an earth-bound terminal with a space vehicle. It is therefore convenient to categorize space channels on the basis of the dominant geometrical and dynamic features of segments of the vehicle trajectory traversed relative to the earth-bound station. On this basis we distinguish the following types of space channels:

- The launch-phase channel
- The near-earth orbital channel
- The near-earth maneuvers channel
- The earth-to-lunar transfer channel
- The lunar-anchored channel
- The interplanetary (or deep-space) channel
- The atmospheric re-entry channel
- The earth terminal-impact channel

Various disturbances dominate during the various phases of a space mission. However, the additive disturbances may be expected to be common to all phases of the mission, although disturbances intercepted by the spacecraft from earth-based equipment not directly beamed at it may be expected to become negligible as the distance from the earth's surface increases. The earth's atmospheric effects are present in all cases and depend in each case on the length and orientation of the path traversed in the atmosphere between ground station and spacecraft. Earth environment additive noises are also common to all in their effect upon the ground terminal, and can only be reduced by proper earth terminal siting and planning.

The above types of transmission channels will now be considered separately in order to bring out their peculiar disturbances.

The Launch-Phase Channel During the launch phase the following propagation disturbances may affect signal transmission significantly:

Booster, ullage and retro-exhaust plasmas introduce severe attenuation, depolarization and phase disturbances by turbulent absorption, refraction and reflection of the desired signal. The booster flame attenuation and attendant severe fluctuations depend upon the aft aspect angle of the rocket.

In the Saturn test series,^{1,2} measurements of signal strength on various links in the 200-Mc and 2000-Mc frequency regions show consistently a dependence of flame attenuation upon aft aspect angle as illustrated in Fig. 1. For aft aspect angles of about 18° or less, the signal strength falls rapidly to a peak attenuation in excess of 20 db at an angle of about 14°, and then builds up again. (Because of prior engine cutoff, no readings on attenuation have been made for aspect angles down to 0°.)

Ullage and retro-rocket effects, however, appear to be independent of aspect angle because the plasma tends to engulf the vehicle. Signal strength recordings illustrating the attenuation caused by the rocket exhausts are shown in Figs. 2 to 4. It is important to observe that the maximum measured attenuation in Fig. 4 is limited in each case by the available signal strength above the receiver noise.

Spectral analysis ² of the fluctuations (with receiver AGC disabled and proper provisions made for avoiding saturation) reveals a nearly uniform spectral density at frequencies below 1 kc, with a rapid cutoff to negligible levels above 3 kc.

Antenna ionization effects have also been observed as the missile traverses altitudes between 40 miles and 60 miles (containing the E layer of the ionosphere) which may account for the fluctuations between 190 and 250 sec in Fig. 2. The antenna RF glow discharge through the ionized layer causes a sharp decrease in signal strength simultaneously at all receiving stations regardless of aspect angle. The attenuation also lifts off simultaneously at all stations as the rocket rises above approximately 60 miles. The effects of ionization discharge include not only a reduction in transmitted power, but also major changes in antenna pattern, impedance and matching characteristics. Evidently, ionization effects can be reduced by reducing the RF power output of the vehicle-borne transmitter. Pressure shock waves at speeds above Mach 1 can also cause signal strength reduction due to fluctuating cancellation of the direct wave by a reflected wave from the surface of the pressure shock wave. ³ The effects upon the signal have been observed, to cause the ground antenna pointing servos to be disturbed sufficiently to steer the antenna beam off the target.

Multipath effects may also be expected during this early phase of the mission, especially when the vehicle is tracked to elevation angles below 10°. Multipath will be considered in some detail in the section on Multipath Effects.

Atmospheric absorption and refraction phenomena will also be present with effects that depend upon the thickness of atmosphere penetrated. Ray bending and changes of phase velocity, principally in the troposphere, affect principally the tracking accuracy.

The launch phase is also characterized by high dynamic range of signal strength and by non-negligible ground-environment additive disturbances at the vehicle.

The Near-Earth Orbital Channel The near-earth orbital channel is characterized by periods of high dynamics in which severe requirements are imposed on acquisition circuits and on techniques for accomplishing handover as the vehicle sets at one station and rises at another. Transmission to and from the spacecraft will be subject to severe multipath at elevation angles below about 5°, and to the effects of absorption and refraction in the atmosphere. The earth environment additive noise may also be occasionally non-negligible at the spacecraft.

The Near-Earth Maneuvers Channel Between the earth parking orbit phase and earth-to-outer space insertion, a number of critical operations and maneuvers may be

necessary. In the Apollo mission, these maneuvers will include CSM/LEM transposition. There are several rocket firings that can cause exhaust plasma effects similar to those described above for ullage and retros.

The Earth-to-Lunar Transfer Channel While the spacecraft is traversing the trajectory leading to or from the vicinity of the moon, the transmission characteristics are expected to portray the gross features of the deep space channel. Normally, it is assumed that the deep space channel is characterized by single-path transmission to the spacecraft, and the changing attenuation with distance is the principal propagation effect (together with the atmospheric absorption and refraction effects, of course). However, the possibility of multipath cannot in general be ruled out, as we shall point out in the section on the Interplanetary (or Deep Space) Channel, below.

The Lunar-Anchored Channel In addition to the expected rocket firings near the moon, transmission to the vicinity of the moon will feature components of signal reflected and scattered off the jagged surface of the moon.

The Interplanetary (or Deep Space) Channel In links between the earth and a spacecraft hundreds of thousands of miles away, at least one terminal (the earth terminal) must use a very high-gain antenna (with a current practical limit on gain of between 60 and 70 db). The beamwidths of such antennas are in moderate to small fractions of degrees. Consequently, small fluctuations in the angle between the axis of the main beam and the direction of arrival of an incident wave can cause either terminal in the receive mode to experience considerable fluctuations in signal level. The angular fluctuations can result from mechanical causes, such as wind pressures and vibrations, or from variable refractive effects in the intervening medium between the two terminals.

Experimental evidence indicates that outer space, especially within the inner regions of the solar system, is far from truly “free space.” The sun’s corona extends at least as far as the earth’s orbit, and considerable ion densities exist in non-uniform distributions. The inherent dispersion in this medium is not considered of practical concern because estimates of the coherence bandwidth are in the hundreds of megacycles for operating frequencies in the 1 to 10Gc range. But the possibility of multipath resulting from deflection at the surfaces of ion blobs of very large dimensions cannot be ruled out, and such multipath has reportedly been experienced already. 4 The differential time delay $\Delta\tau$ between a direct path and a secondary path, with a small difference θ in angle of arrival from a transmitter a distance R away, may be about $R\theta^2/2c$ for deflection at very small grazing angles near midpath, where c is the velocity of light. If $\theta = 10^{-3}$ rad, $\Delta\tau$ will be in microseconds for values of R in millions of kilometers.

The Atmospheric Re-entry Channel Re-entry into the earth's atmosphere is distinguished by high dynamics and by the formation of an intense plasma sheath enveloping the re-entering spacecraft. Total blackout is an almost certain occurrence for the duration of the plasma sheath. In addition, the trailing plasma as well as the large volume of the enveloping plasma will have a strong effect on target acquisition and definition by skin-tracking radars.

The Earth Terminal-Impact Channel Prior to terminal impact, reception from the spacecraft by ground stations and by aircraft may experience significant multipath effects.

Plasma Effects There are several critical intervals in the life of a space mission when rockets are fired giving rise to exhaust plasma clouds. The times of these firings are times when a command may be desired to trigger some critical operation, and continued reliable telemetry transmission is essential for later diagnosis of possible malfunctions. For example, in the earlier phases of a Saturn V lunar shot, out to 25,000 miles, there is the large booster rocket on takeoff. Later, retros are fired to separate S-IC from the rest of the rocket system. This is preceded by ullage rockets for compressing the fuel by a gravitational-type pressure in order to aid the fuel pumps in igniting the S-II stage. The same is repeated when separating S-II from S-IVB and igniting S-IVB, when separating S-IVB from the spacecraft, and in later maneuver operations to direct the spacecraft out toward the moon.

Vehicles moving at hypersonic speeds through the atmosphere also become engulfed in a plasma caused by the intense heat of friction.

The plasmas that form in the trailing rocket exhaust region during powered phases of flight and rocket-powered maneuvers, and around a vehicle in hypersonic motion during atmospheric exit and re-entry are in general highly turbulent. Signals impinging on such dense, nonuniform and highly turbulent plasmas experience nonlinear randomly time-variant effects.

In response to an applied electromagnetic field, the vibrating electrons in the plasma act as parasitic radiators alternately absorbing and re-radiating energy. Collisions introduce a randomizing effect that keeps the excited plasma from re-radiating coherently with the applied field. The net effect of this turbulent randomization is to cause a signal attenuation, signal frequency spread, spurious modulations, loss of phase coherence between signals, and a change of polarization. Plasmas also strongly affect antenna matching characteristics, radiation patterns, and power handling capability, and reduce the field strength necessary for breakdown in the aperture region. Breakdown is a condition in which the air surrounding the antenna aperture becomes a strongly

conducting medium that will not support wave propagation. Antenna breakdown is a very common cause of telemetry, command, and communication dropout. The absorption of energy by the plasma from the radio waves also provides a nonlinear response that causes cross-modulation and frequency mixing among two or more strong signals present.

Unfortunately, no data are available at present that would enable us to estimate the signal distorting characteristics of the plasma "filter." It is known, however, that at frequencies exceeding the plasma frequency, where the plasma behaves essentially as a dielectric, a nonturbulent plasma propagates a signal with negligible attenuation and) although it shifts the signal phase, it does not affect noticeably the mutual coherence properties of the signal components. But records of signal envelope behavior gathered on test firings indicate that signals in the 200-500 Mc range undergo severe attenuation, characteristic of operation below the plasma frequency. Attenuation ranging between 10 and 30 db is observed in the ascent phase of the flight. Blackouts extending up to 6 sec accompany retrofirings with observed attenuation of up to 60 db. Exhaust plasmas of solid-fuel engines (such as the retro-rockets in the Saturn tests) introduce more severe effects than those of liquid-fuel engines. Moreover, the rapidly fluctuating noise-like appearance of recorded envelopes caused by the plasma indicates a high degree of turbulence and suggests that considerable intermodulation and phase randomization effects would emerge among the components of a signal. Experimental studies of the fluctuations in signal strength caused by exhaust plasmas of the Saturn vehicle thus far show a power spectral density that is uniform for frequencies below 1 kc, and cuts off rapidly to negligible levels beyond 3 kc.

Quantitative predictions of the exhaust plasma effects require specification of the carrier frequency, ω , the length x of the traversed path, the electron density profile, $N(x)$, along the traversed path, and the collision frequency ν as a function of x . The transmission loss can then be expressed as

$$A(h) \approx K \frac{1}{\omega^2} \int_0^X N(x)\nu(x) dx \quad \text{in db} \quad (1)$$

where K is a constant and $A(h)$ is, in general, a function of altitude, h .

For a mission requiring a variable thrust, all of the above parameters will change rapidly, in a way that, in principle at least, can be predicted if the following are known: thrust profile, propellant, nozzle material and configuration, nozzle pressure and temperature, ambient conditions, and contaminants. Similar information will be required for the prediction of any other effects. To predict, for instance, the nonlinear mixing of two signals, one needs, in addition, to know the near-zone field strength, the local electron

temperature and the collision parameters peculiar to the chemical compounds present. The complexity of relating the required basic information to the gross effects upon the signal and the difficulty in obtaining the basic information even in well specified cases makes reasonably close quantitative predictions of plasma effects nearly impossible at the present time.

Some general statements can however be made of a rather qualitative nature. For example, it is reasonable to expect that unless the transmission is blacked out because of antenna breakdown or total opacity, the signal emerging through the plasma may be modeled by a pure scatter component with the properties of a complex gaussian process superimposed on a “specular” component of comparable or larger mean-square value. This may be justified by heuristic reasoning in terms of the mechanism of interaction of the incident signal and the turbulent plasma below the plasma frequency, and in terms of the Central Limit Theorem.

Three gross parameters of the transmission are usually of special interest to the system designer. The first, called the coherence bandwidth, defines the maximum range of frequencies over which all frequency components would fluctuate essentially in step, or the fading is essentially frequency-flat. The second, usually called the fading bandwidth, defines the nominal width of the dispersion in frequency suffered by each individual frequency component; or, equivalently, is defined by the nominal rate at which the fluctuations in the channel occur. The third, which we call the diversity bandwidth, or the decorrelation bandwidth, is the minimum frequency separation between two input carriers that will result in a correlation coefficient of $1/e$ or less between the corresponding output envelopes. For propagation through a plasma, these parameters depend on the path length, the conditions of the intervening plasma and the mechanism of multipath transmission in the presence of the plasma. The time variability of the geometry of the propagation paths in the link and the turbulence of the plasma account for the fluctuations in the multipath conditions that degrade system performance. Thus, the above parameters are themselves random variables that, strictly speaking, can only be specified in statistical terms.

Generally speaking, one can only state broad guidelines for design estimation of the above parameters at the present time. Thus, the definition of coherence bandwidth must be based on a criterion of performance degradation that is suitable for the intended application. Computations based on reasonable engineering criteria of noticeable degradation in probability of error of binary signal reception and intermodulation distortion of FDM/FM signals, show that the coherence bandwidth should be taken as roughly one tenth or less of the reciprocal of the difference between the times of arrival of the earliest and the latest significant paths. The diversity bandwidth is about 10 to 50 times the coherence bandwidth. The fading bandwidth experienced to date in the Saturn test series is between 1 and 2 kc.

Illustrations of multipath mechanisms associated with an exhaust plasma are shown in Fig. 5. In Fig. 5(a) the spatial selectivity of the ground transmitting and receiving antenna, as defined by a beamwidth α_{GA} , limits the angular spread of the main-beam receivable paths at the ground antenna. In Fig. 5(b) the dimensions of the trailing exhaust region limit the maximum angular spread of the main-beam receivable paths. In each case, all but a direct unobstructed path can be expected to portray a fine structure caused by the turbulence of the plasma. Estimates of the delay spread of the paths can be made in each case for estimating coherence bandwidths.

Thus, for the configuration of Fig. 5(a), the maximum differential path delay is approximately

$$\tau_{d, \max} \approx \frac{h(h-a)}{2ca} \alpha_{GA}^2 \quad (\approx \frac{h^2}{2ca} \alpha_{GA}^2 \text{ for } h \gg a) \quad (2)$$

where a is the distance, along the direct path, from the vehicle antenna to the perpendicular from the reflection point. Thus

$$B_{\text{coh}} \lesssim 2ca / [10 \alpha_{GA}^2 h(h-a)] \quad (\approx 2ca / 10 \alpha_{GA}^2 h^2, \text{ for } h \gg a) \quad (3)$$

For a 1° beamwidth,

$$B_{\text{coh}} \lesssim 200 a/h^2 \text{ Mc for } h \text{ and } a \text{ in km, and } h \gg a$$

For the situation illustrated in Fig. 5(b) the width of the delay spread is approximately

$$\tau_{d, \max} \approx \frac{h(h-a)}{2ca} \left(\frac{D}{h-a} \right)^2 = \frac{D^2 h}{2ca(h-a)} \quad (4)$$

where D is the maximum diameter of the plume and a is defined for the extreme secondary ray as in Eq. (2), the reflection point being taken at the final deflection that directs the ray to the ground antenna. The corresponding B_{coh} is estimated to be

$$B_{\text{coh}} \lesssim 2ca(h-a) / 10 D^2 h \quad (\approx \frac{2ca}{10 D^2} \text{ for } h \gg a) \quad (5)$$

Thus, for $D = 300$ m, and $h \gg a$,

$$B_{\text{coh}} \lesssim 0.6 a \text{ Mc for } a \text{ in km}$$

An estimate of coherence bandwidth may also be given for forward scattering through a plasma. Such estimates depend upon the dimensions of the irregularities, blobs, or turbulent eddies in the plasma. In forward scattering, only the irregularities of the largest

scale ($2\pi L/\lambda > 1$) are of importance.⁵ For a weak scattering case (multiple reflections neglected) it can be shown⁶ that the fractional correlation bandwidth is, approximately,

$$B_{\text{corr}} \approx \frac{L^2 f^2}{\pi h c} \quad (6)$$

where h is the distance of the irregularities from the receiver and c is the velocity of light. By definition, the correlation bandwidth in this formula is the frequency separation B_{corr} between two incident carriers at which the cross-correlation function between the envelopes of the responses to these carriers falls to one-half. The coherence bandwidth should be taken as about one-tenth or less of the correlation bandwidth. Accordingly, we write

$$B_{\text{coh}} \lesssim \frac{L^2 f^2}{10 \pi h c} \quad (7)$$

As an illustration, if $L = 30$ m and $h = 5 \times 10^4$ m, then

$$\begin{aligned} B_{\text{coh}} &\lesssim 8 \text{ Mc} \quad \text{for } f = 2000 \text{ Mc} \\ &\lesssim 500 \text{ kc} \quad \text{for } f = 500 \text{ Mc} \end{aligned}$$

It is interesting to point out that the presence of the plasma near to or engulfing the receiving antenna contributes to the operating noise temperature of the receiving system. It has been shown⁷ that for an isotropic plasma around a hyper-velocity vehicle, the excess noise temperature results mainly from

- a) the vehicle surface temperature for radio frequencies below the plasma frequency (the vehicle surface contributing about 500°K , the plasma $100\text{-}200^\circ\text{K}$);
- b) external sources for radio frequencies well above the plasma frequency (e. g. , 300°K by the earth's surface, plus a rapidly decreasing contribution of less than 100°K from the plasma); and
- c) direct emission by the plasma for radio frequencies about the plasma frequency (with a pronounced peak of about 2000°K from the plasma alone just above the plasma frequency).

6.0 Multipath Effects A variety of propagation mechanisms gives rise to secondary-path signals. It is convenient to distinguish between

- a) deflection mechanisms including scattering, path splitting, ducting and critical reflections at boundaries of regions with nonuniform and rapidly changing refractive properties in the intervening atmosphere and outer space; and

- b) reflections at earth (land or water) and lunar surfaces and intervening massive obstacles.

Secondary paths, ranging between specular and diffuse, depending upon the secondary transmission medium, are received because of insufficient transmitting and/or receiving antenna directivity and because of minor lobes. Multipath of type (a) may dominate principally in links with highly directive antennas oriented at elevation angles greater than one-half the beamwidth above potential reflecting surfaces or obstacles. Reflected secondary paths may always be received through minor lobes, but dominate in major lobe reception at low elevation angles when the antenna beam intercepts ground surfaces and obstacles.

The two-path case may in general occur more frequently than the case of more than two paths. The relative path strengths and differential delays are critical parameters. Let $f_g(\theta_h, \theta_v)$ define the ground antenna pattern (relative to the direction of maximum transmission $\theta_h = 0, \theta_v = 0$), and $f_s(\theta_p, \theta_c)$ define the vehicle antenna pattern (θ_p denotes angle in the radial plane through the central axis of the missile, θ_c angle in the plane perpendicular to the missile axis). The relative amplitude of the reflected wave at the receiver, as compared with the direct wave, will be the reflection coefficient multiplied by the excess path loss and by

$$\gamma \equiv \frac{f_g(\theta_{h,2}, \theta_{v,2}) f_s(\theta_{p,2}, \theta_{c,2})}{f_g(\theta_{h,1}, \theta_{v,1}) f_s(\theta_{p,1}, \theta_{c,1})}$$

in which the subscripts 1 and 2 represent the direct and the reflected paths respectively.

The worst reflections are usually from a large body of water. For reflection from a body of water, the surface roughness will not generally be sufficient to result in a reduction of the reflection coefficient to a low level, except perhaps in rough weather with exceptionally high winds. The reflection is therefore often essentially specular and very bad fades can always be expected, especially with horizontally polarized waves. But with vertically polarized waves the reflection coefficient, though very nearly equal to unity for very small grazing angles, drops to about 0.7 for grazing angles near 1° , which may lead to significantly shallower fades (especially at the lower microwave frequencies) than is experienced with horizontally polarized waves.

The amplitude ratio of reflected to direct path is thus a function of polarization, the characteristics of the reflecting surface, the various orientation angles indicated in the above expression for γ , the grazing angle, etc. (For grazing angles below 1° , the reflection coefficient of reflecting surfaces is almost independent of the conductivity and

dielectric properties of the surface, the polarization of the wave, and the grazing angle. The principal controlling factor is then the surface roughness.) It is therefore difficult to give numerical examples without being too specific. But some general observations can be made:

Amplitude ratios close to unity are likely, and differential path delays of up to a few milliseconds may be encountered. But high amplitude ratios will most frequently be associated with differential path delays of a few microseconds or less. Under most other practical conditions in the AMR area, one may expect amplitude ratios near unity to be associated with delay differences of less than 1 μsec , and delay differences of the order of 10 μsec or more to be associated with amplitude ratios of a few tenths or less. In air-to-air links, where telemetry signals are received in an aircraft at altitudes of several miles and reflection occurs at a water surface, delay differences of 10 μsec or more may be encountered with amplitude ratios between 0.5 and 1.

Envelope fluctuations of about 10 db have been observed within the first few minutes after take-off, indicating amplitude ratios of over 0.8 and delay differences of less than 1 μsec .

For purposes of system-function characterization of the channel, we recognize the following facts:

- i) The most common case of multipath is one in which two replicas of the desired signal are received.
- ii) More than two replicas of the desired signal are sometimes encountered, and not too infrequently.
- iii) At elevation angles near zero degrees somewhat localized, frequency-selective deep fades may be brought about by the interaction of a few components, perhaps four to six. Among these components, those with relatively long delays usually are appreciably smaller in magnitude than those with shorter delays. The relatively weak and longer delayed components are important in determining the shape of the path-loss versus frequency curve near the maxima of loss. Deep fades resulting from multipath on links with adequate path clearance are always frequency selective with near-Rayleigh fading statistics. A steady relatively non-selective component of loss of about 10 db usually accompanies frequency-selective deep fades.
- iv) The various received replicas have different angles of arrival in the vertical plane, usually fractions of a degree above the line-of-sight for atmospheric multipath, fractions of a degree below the line-of-sight for ground and water surface reflections

and sometimes for atmospheric multipath as, for example, under substandard atmospheric conditions causing upward bending of the rays.

- v) The atmospheric multipath propagation characteristics appear to be independent of polarization.

If we assume truly specular paths, the resultant signal $y(t)$ at the receiving end, in response to $x(t)$ at the transmitting end may, in general, be expressed as

$$y(t) = \sum_{n=1}^N a_n x(t - \tau_{d,n}) \quad (8)$$

where $\tau_{d,n}$ is the transmission delay of the n^{th} path, and a_n is the associated attenuation factor. If the a_n 's are properly defined, this expression holds independently of whether or not each path results in distortionless transmission of $x(t)$ (i.e., whether or not the individual paths provide uniform attenuation and linear phase shift across the frequency band occupied by $x(t)$). If $x(t)$ is of sufficiently short duration, then the a_n 's and $\tau_{d,n}$'s will be relatively time-invariant over the duration of $x(t)$, and we can write

$$Y(j\omega) = X(j\omega) \sum_{n=1}^N a_n e^{-j\omega\tau_{d,n}} \quad (9)$$

The system function of the line-of-sight transmission medium may therefore be expressed in the form

$$H(j\omega, t) = \sum_{n=1}^N a_n(t) e^{-jn\omega\tau_{d,n}(t)} \quad (10)$$

in which the dependence of a_n and $\tau_{d,n}$ upon time is explicitly brought out. This representation holds as long as the channel fluctuations are slow relative to the data-bearing fluctuations in the signal parameters.

For purposes of illustration, consider the likely case in which only two paths are important. Here

$$H(j\omega, t) = a_1(t) e^{-j\omega\tau_{d,1}(t)} + a_2(t) e^{-j\omega\tau_{d,2}(t)} \quad (11)$$

The channel is then modeled as in Fig. 6. A phasor construction of $H(j\omega, t)$ is shown in Fig. 7. This resultant phasor operates on the transmitted signal. Zeros of transmission will occur if

$$a_1 = a_2$$

and

$$\omega\tau_1 = \omega\tau_2 + (2n + 1)\pi, \quad n = 0, 1, 2, \dots$$

or

$$\omega = \frac{(2n + 1)\pi}{(\tau_1 - \tau_2)}, \quad n = 0, 1, 2, \dots$$

Figure 8 gives a plot of $|H(j\omega, t)|$ of Eq. (11) as a function of ω for fixed t , and for different values of $a \equiv a_2/a_1$. With changes in time delays and additional paths, one obtains the classical selective fading effects.

Effect of Two-Path Propagation on FDM/EM Reception The type of signal employed most frequently in space instrumentation and communication links consists of a number of frequency-division multiplexed subchannels that frequency- or phase-modulate the radio-frequency carrier. For convenience, we shall refer to this class of signals as FDM/EM signals, EM denoting exponent modulation (FM or PM) of the RF carrier. It is instructive to explore the effects of two-path reception of FDM/EM signals.

Let the FDM/EM signal arriving via the direct path be represented at the output of the receiver IF by

$$e_1(t) = E_s \cos[\omega_c t + \psi(t)] \quad (13)$$

in which

$$\begin{aligned} \psi(t) &= \Delta\Phi g(t) && \text{for PM} \\ \psi(t) &= \Delta\Omega \int_t^t g(\eta) d\eta && \text{for FM} \end{aligned} \quad (14)$$

$$\begin{aligned} g(t) &= \text{sum of frequency-division multiplexed} \\ &\quad \text{subchannel waveforms normalized} \\ &\quad \text{so that } |g(t)|_{\max} = 1 \end{aligned}$$

and

$$\Delta\Phi = \text{phase deviation, in radians of the RF carrier}$$

$$\Delta\Omega = \text{frequency deviation, in rad/sec}$$

As stated in the previous section, the most likely case of multipath disturbance is one in which only a second path is received of amplitude aE_s ($a < 1$) and delay difference τ_d (ranging up to a few tens of microseconds), with a and τ_d substantially constant over hundreds of cycles of the lowest-frequency subcarrier. Thus, under this condition of multipath transmission, the resultant signal at the output of the receiver IF amplifier is

$$\begin{aligned}
e_{if}(t) &= E_s \{ \cos [\omega_c t + \psi(t)] + a \cos [\omega_c (t - \tau_d) + \psi(t - \tau_d)] \} \\
&= E_s A(t) \cos [\omega_c t + \psi(t) + \theta(t)]
\end{aligned} \tag{15}$$

where

$$A(t) = \sqrt{1 + a^2 + 2a \cos \phi(t)} \tag{16}$$

$$\theta(t) = \tan^{-1} \frac{a \sin \phi(t)}{1 + a \cos \phi(t)} \tag{17}$$

and

$$\phi(t) = \omega_c \tau_d + \psi(t) - \psi(t - \tau_d) \tag{18}$$

In order to bring out the nature and level of distortion contained in $\theta(t)$ we shall consider first modulation by a single unmodulated subcarrier, and second modulation by a sum of sinewaves. For this purpose, it is convenient to express $\theta(t)$ in the form

$$\begin{aligned}
\theta(t) &= \text{Im} \{ \ln [1 + a e^{j\phi(t)}] \} \\
&= \text{Im} \left\{ - \sum_{n=1}^{\infty} \frac{(-a)^n}{n} e^{jn\phi(t)} \right\}, \quad a^2 < 1
\end{aligned} \tag{19}$$

The analysis will be aimed at illustrating the nature and level of the base band harmonic and intermodulation distortion products - of importance in telemetry and other FDM instrumentation - , and the phase shifts acquired by the subchannel tones - of principal importance in sidetone ranging systems.

Carrier Modulation by One Sinewave Consider first carrier modulation by a single subcarrier expressed as

$$\psi(t) = \delta \sin(\omega_m t + \phi_m), \quad \delta \equiv \Delta\Omega / \omega_m \text{ for FM} \tag{20}$$

This special case has been studied theoretically by Corrington⁷, and experimentally by Becker⁸. Our analysis here provides additional insight and bounds on important effects.

Substitution from Eg. (20) into (18) yields

$$\begin{aligned}
\phi(t) &= \omega_c \tau_d + \delta \{ \sin(\omega_m t + \phi_m) - \sin[\omega_m (t - \tau_d) + \phi_m] \} \\
&= \omega_c \tau_d + \delta_d \sin(\omega_m t + \phi_m + \phi_d)
\end{aligned} \tag{21}$$

where

$$\delta_d = 2\delta \sin(\omega_m \tau_d / 2) \quad (22)$$

and

$$\phi_d = -(\omega_m \tau_d - \pi) / 2 \quad (23)$$

Substitution into Eq. (19) followed by use of the identity

$$e^{jx \sin \beta} = \sum_{k=-\infty}^{\infty} J_k(x) e^{jk\beta}$$

where $J_k(x)$ is the Bessel function of the first kind, k^{th} order and argument x , leads to

$$\theta(t) = - \sum_{k=-\infty}^{\infty} \sum_{n=1}^{\infty} \frac{(-a)^n}{n} J_k(n\delta_d) \sin[k\omega_m t + k(\phi_m + \phi_d) + n\omega_c \tau_d], \quad a^2 < 1 \quad (24)$$

If an ideal frequency demodulator is assumed, the output prior to filtering by any baseband subchannel filters is proportional to

$$\begin{aligned} \omega_c(t) &= \dot{\psi}(t) + \dot{\theta}(t) \\ &= \Delta\Omega \cos(\omega_m t + \phi_m) - \sum_{k=-\infty}^{\infty} \sum_{n=1}^{\infty} k\omega_m \frac{(-a)^n}{n} J_k(n\delta_d) \cos[k\omega_m t \\ &\quad + k(\phi_m + \phi_d) + n\omega_c \tau_d], \quad a^2 < 1 \\ &= \Delta\Omega \cos(\omega_m t + \phi_m) + \sum_{k=1}^{\infty} D_k(t) \end{aligned} \quad (25)$$

where

$$D_k(t) = -2k\omega_m \left[\sum_{n=1}^{\infty} \frac{(-a)^n}{n} J_k(n\delta_d) \cos(n\omega_c \tau_d) \right] \cos k(\omega_m t + \phi_m + \phi_d) \quad \text{for } k = 1, 3, 5, \dots \quad (26)$$

$$\equiv 2k\omega_m \left[\sum_{n=1}^{\infty} \frac{(-a)^n}{n} J_k(n\delta_d) \sin(n\omega_c \tau_d) \right] \sin k(\omega_m t + \phi_m + \phi_d) \quad \text{for } k = 2, 4, 6, \dots \quad (27)$$

Equations (24) and (25) clearly show that the presence of the second path gives rise to phase or frequency modulation distortion terms at the frequency of the modulating subcarrier and at all harmonics of it. Of particular interest here is the distortion term that coincides in frequency with the desired subcarrier. This term is given by

$$D_1(t) = - \left[2\omega_m \sum_{n=1}^{\infty} A_{1,n}(a, \delta, \omega_c \tau_d) \right] \cos(\omega_m t + \phi_m + \phi_d) \quad (28)$$

where

$$A_{1,n}(a, \delta, \omega_c \tau_d) \equiv \frac{(-a)^n}{n} J_1(n\delta_d) \cos(n\omega_c \tau_d) \quad (29)$$

This fundamental distortion term is seen to differ in phase from the desired subcarrier term by $\phi_d - \pi = -(\omega_m \tau_d + \pi)/2$. The resultant subcarrier component will therefore have a phase error given by

$$(\text{Phase Error}) = -\tan^{-1} \frac{\gamma_1 \cos(\omega_m \tau_d/2)}{1 - \gamma_1 \sin(\omega_m \tau_d/2)} \quad (30)$$

where

$$\gamma_1 \equiv (2/\delta) \sum_{n=1}^{\infty} A_{1,n}(a, \delta, \omega_c \tau_d), \quad a^2 < 1. \quad (31)$$

The infinite series in Eq. (31) as well as those for the evaluation of the harmonic distortion components in Eqs. (26) and (27) converge rather slowly for values of a nearing unity. However, since we are mainly interested in order-of-magnitude estimates, it is interesting to observe that

$$|A_{1,n}(a, \delta, \omega_c \tau_d)|_{\max} < 0.6 \frac{a^n}{n}$$

(the value of $A_{k,n}$ for the k^{th} harmonic may be similarly bounded) so that

$$|\gamma_1|_{\max} < \frac{1.2}{\delta} \sum_{n=1}^{\infty} \frac{a^n}{n} = -\frac{1.2}{\delta} \ln(1 - a), \quad a^2 < 1 \quad (32)$$

Therefore, from Eq. (30) we have

$$|(\text{Phase Error})| < \left| \tan^{-1} \frac{\cos(\omega_m \tau_d/2)}{\delta/[1.2 \ln(1 - a)] + \sin(\omega_m \tau_d/2)} \right| \quad (33)$$

In view of the fact that negative and positive quantities are summed in the expression for γ_1 and only the magnitudes of these quantities are considered in Eq. (32), the upper bounds in Eqs. (32) and (33) are not expected to be sufficiently tight to make them useful

in obtaining realistic estimates of $|\gamma_1|_{\max}$ and of the maximum phase error. But for values of the parameters involved that yield small values for the bounds, it is useful to know that even the most pessimistic estimates of $|\gamma_1|_{\max}$ and of the phase error would be that small.

Carrier Modulated by Sum of Several Sinewaves In most applications, the subchannel signals can be modeled by single sinewaves for preliminary assessment of disturbances. Thus we set

$$\dot{\psi}(t) = \sum_{\ell=1}^N (\Delta\Omega)_{\ell} \cos(\omega_{sc,\ell} t + \phi_{sc,\ell}) \quad (34)$$

in which we may consider the various $\omega_{sc,\ell}$ components to represent different unmodulated subcarriers or to be bunched into subgroups that occupy relatively small bands near nominal subcarrier frequencies, each subgroup representing a particular subchannel signal. We define

$$\delta_{\ell} \equiv \frac{(\Delta\Omega)_{\ell}}{\omega_{sc,\ell}} \quad (35)$$

Substitution of

$$\psi(t) = \sum_{\ell=1}^N \delta_{\ell} \sin(\omega_{sc,\ell} t + \phi_{sc,\ell}) \quad (36)$$

into Eq. (18) yields

$$\dot{\phi}(t) = \omega_c \tau_d + \sum_{\ell=1}^N \delta_{\ell,d} \sin(\omega_{sc,\ell} t + \phi_{sc,\ell} + \phi_{d,\ell}) \quad (37)$$

where

$$\delta_{\ell,d} \equiv 2 \delta_{\ell} \sin(\omega_{sc,\ell} \tau_d / 2) \quad (38)$$

and

$$\phi_{d,\ell} \equiv -(\omega_{sc,\ell} \tau_d - \pi) / 2 \quad (39)$$

Therefore, in the present case

$$\begin{aligned}
 e^{jn\phi(t)} &= e^{jn\omega_c \tau_d} \cdot \exp \sum_{\ell=1}^N n\delta_{\ell,d} \sin(\omega_{sc,\ell} t + \phi_{sc,\ell} + \phi_{d,\ell}) \\
 &= e^{jn\omega_c \tau_d} \prod_{\ell=1}^N \left[\sum_{k_\ell=-\infty}^{\infty} J_{k_\ell}(n\delta_{\ell,d}) e^{jk_\ell(\omega_{sc,\ell} t + \phi_{sc,\ell} + \phi_{d,\ell})} \right]
 \end{aligned}$$

Consequently, the output of an ideal frequency demodulator prior to any baseband subchannel filtering will be proportional to

$$\begin{aligned}
 \omega_i(t) &= \sum_{\ell=1}^N (\Delta\Omega)_\ell \cos(\omega_{sc,\ell} t + \phi_{sc,\ell}) \\
 &- \sum_{n=1}^{\infty} \frac{(-a)^n}{n} \left\{ \sum_{k_1=-\infty}^{\infty} \dots \sum_{k_N=-\infty}^{\infty} \left[\prod_{\ell=1}^N J_{k_\ell}(n\delta_{\ell,d}) \right] \left(\sum_{\ell=1}^N k_\ell \omega_{sc,\ell} \right) \right. \\
 &\left. \cos \left[\left(\sum_{\ell=1}^N k_\ell \omega_{sc,\ell} \right) t + \sum_{\ell=1}^N k_\ell (\phi_{sc,\ell} + \phi_{d,\ell}) + n\omega_c \tau_d \right] \right\} \quad (40)
 \end{aligned}$$

This awesome expression brings out the important fact that the presence of the second path introduces nonlinear interactions among the multiplexed baseband subchannels. Thus there will be interaction terms at all frequencies that result from the linear combination

$$k_1 \omega_{sc,1} + k_2 \omega_{sc,2} + \dots + k_N \omega_{sc,N} \quad (41)$$

in which k_ℓ , for each integer ℓ from 1 to N , ranges over all integers from $-\infty$ to $+\infty$.

The result expressed in Eq. (40) may actually be interpreted in at least two important ways for the present application. First, with the frequencies, $\omega_{sc,\ell}$, considered as representative of multiplexed subcarriers, Eq. (37) brings out the cross-modulation by-products among the subcarriers. Some of these may fall within frequency spaces allotted for the various subcarriers and will then cause interference with those subcarriers. Second, if the various $\omega_{sc,\ell}$ frequencies are grouped into a few subgroups, and each of the subgroups is considered to represent a subchannel signal, it becomes clear that beats among the components of each subchannel and their harmonics will occur. Since the components of each individual subchannel signal will be of nearly equal frequencies, beats among them and among their harmonics will have frequencies down in the vicinity of zero frequency. Since every subchannel signal will contribute such beats, a ‘‘pile up’’ of distortion products may be expected down in the region near zero frequency and

extending from 0 cps at least over a small multiple of the nominal bandwidth of a typical subchannel. These distortion products should be carefully evaluated in the design of subchannel signals for occupying that region of the spectrum.

Special Case of Small \underline{a} The above results may be greatly simplified in the special case in which the amplitude ratio \underline{a} is less than about 0.1. First we observe that

$$\begin{aligned}\theta(t) &= \tan^{-1} \frac{a \sin \phi(t)}{1 + a \cos \phi(t)} = a \sin \phi(t) - \frac{1}{2} a^2 \sin 2 \phi(t) \\ &\quad + \frac{1}{3} a^3 \sin 3 \phi(t) - \dots \\ &\approx a \sin \phi(t) \text{ for all } \underline{a} \leq 0.2\end{aligned}\quad (42)$$

From Eq. (42) we have

$$\begin{aligned}\dot{\theta}(t) &= -\dot{\phi}(t) \sum_{n=1}^{\infty} (-a)^n \cos n \phi(t) \\ &\approx a \dot{\phi}(t) \cos \phi(t) \text{ if } \underline{a} \leq 1/10\end{aligned}\quad (43)$$

Under these conditions, an ideal carrier frequency demodulator would deliver an output, prior to subchannel filtering, proportional to

$$\omega_i(t) \approx \dot{\psi}(t) + a \dot{\phi}(t) \cos \phi(t), \quad \underline{a} \leq 1/10 \quad (44)$$

For modulation by a single subcarrier, $\phi(t)$ is given by Eq. (21). By direct substitution and expansion of Eq. (44), or direct use of Eqs. (26) and (27) with n restricted only to unity, as per approximation (43), we have, for $\underline{a} \leq 1/10$,

$$\begin{aligned}D_k(t) &\approx [2 a \omega_m^k J_k(\delta_d) \cos \omega_c \tau_d] \cos k(\omega_m t + \phi_m + \phi_d) \\ &\quad \text{for } k = 1, 3, 5, \dots\end{aligned}\quad (45)$$

$$\begin{aligned}&\approx [2 a \omega_m^k J_k(\delta_d) \sin \omega_c \tau_d] \sin k(\omega_m t + \phi_m + \phi_d) \\ &\quad \text{for } k = 2, 4, 6, \dots\end{aligned}\quad (46)$$

Moreover, in Eq. (28) for the phase error in the resultant fundamental term,

$$\gamma_1 \approx - (2a/\delta) J_1(\delta_d) \cos \omega_c \tau_d \quad (47)$$

Further simplifications may be made for the situations in which $\omega_m \tau_d$ is low. For example, for $\omega_m \tau_d \leq 1.54$ rad,

$$\delta_d = 2\delta \sin(\omega_m \tau_d / 2) \approx \Delta \Omega \tau_d \quad (48)$$

Also, $\cos(\omega_m \tau_d / 2) \approx 1$ for $(\omega_m \tau_d \leq 0.88)$. Consequently, the expression for the phase error of the fundamental term may be approximated by

$$\begin{aligned} \text{(Phase Error)} \approx \tan^{-1} \frac{(2a/\delta) J_1(\Delta\Omega \tau_d) \cos \omega_c \tau_d}{1 + (a/\delta) \omega_m \tau_d J_1(\Delta\Omega \tau_d) \cos \omega_c \tau_d} \\ \text{for } \underline{a} \leq 1/10 \text{ and } \omega_m \tau_d \leq 0.88 \end{aligned} \quad (49)$$

If we add the condition $\delta \geq 0.528$, we can drop the second term in the denominator in Eq. (49). Indeed,

$$\begin{aligned} \text{(Phase Error)} \approx (2a/\delta) J_1(\Delta\Omega \tau_d) \cos \omega_c \tau_d \text{ rad} \\ \text{for } \underline{a} \leq 1/10, \omega_m \tau_d \leq 0.88, \text{ and } \delta \geq 0.528 \end{aligned} \quad (50)$$

Under the restrictions indicated with the approximation in Eq. (50)

$$\begin{aligned} |\text{Phase Error}| < 0.12/\delta \text{ rad} \\ < 7/\delta \text{ degrees} \end{aligned} \quad (51)$$

From Eq. (46) we also have for the amplitude of the second harmonic

$$4 \omega_m a J_2(\delta_d) \sin \omega_c \tau_d, \quad \underline{a} \leq 1/10 \quad (52)$$

which for $\omega_m \tau_d \leq 1.54$ may be approximated by

$$4 \omega_m a J_2(\Delta\Omega \tau_d) \sin \omega_c \tau_d$$

The amplitude of the second harmonic is bounded by $2a\omega_m$ as long as $\underline{a} \leq 1/10$.

In a similar fashion, some approximations can also be made when $\underline{a} \leq 1/10$ for the case in which the carrier frequency is modulated by the sum of several tones. Unfortunately, the permissible approximations do not simplify the appearance of the expressions a great deal. For example, with $\underline{a} \leq 1/10$, the summation over n in Eq. (40) is restricted to $n=1$. For $N=2$ (i.e., only two subcarriers present) and $\underline{a} \leq 1/10$

$$\begin{aligned} \omega_1(t) \approx (\Delta\Omega)_1 \cos(\omega_{sc,1} t + \phi_{sc,1}) + (\Delta\Omega)_2 \cos(\omega_{sc,2} t + \phi_{sc,2}) \\ + a \sum_{k_1=-\infty}^{\infty} \sum_{k_2=-\infty}^{\infty} (k_1 \omega_{sc,1} + k_2 \omega_{sc,2}) J_{k_1}(\delta_{1,d}) J_{k_2}(\delta_{2,d}) \\ \cos[(k_1 \omega_{sc,1} + k_2 \omega_{sc,2}) t + k_1(\phi_{sc,1} + \phi_{d,1}) \\ + k_2(\phi_{sc,2} + \phi_{d,2}) + (\omega_c \tau_d)] \end{aligned} \quad (53)$$

Thus, the distortion terms having the frequencies

$$\omega_{sc,1} \pm \omega_{sc,2} \text{ rad/sec}$$

are given by

$$\begin{aligned} & \mp [2a(\omega_{sc,1} \pm \omega_{sc,2}) J_1(\delta_{2,d}) J_1(\delta_{2,d}) \sin(\omega_c \tau_d)] \\ & \sin[(\omega_{sc,1} \pm \omega_{sc,2})t + \phi_{sc,1} \pm \phi_{sc,2} + \phi_{d,1} \pm \phi_{d,2}] \end{aligned} \quad (54)$$

The amplitudes of these terms are bounded by

$$0.72 a |\omega_{sc,1} \pm \omega_{sc,2}|, \quad \underline{a} \leq 1/10 \quad (55)$$

The second harmonic of the $\omega_{sc,1}$ subcarrier is given by

$$\begin{aligned} & -[4a\omega_{sc,1} J_2(\delta_{1,d}) J_0(\delta_{2,d}) \sin(\omega_c \tau_d)] \sin 2(\omega_{sc,1} t \\ & \quad + \phi_{sc,1} + \phi_{d,1}) \end{aligned} \quad (56)$$

The amplitude of this component is bounded by $2a\omega_{sc,1}$, $\underline{a} \leq 1/10$.

The above results are of special interest in FDM/FM telemetry and in range and range rate tracking employing sidetones. More realistic model of subcarriers using noise loading to simulate voice channels and relative wideband telemetry signals may also be used and the analysis retraced. The analysis is then greatly facilitated by using the fact that powers of time functions lead to spectra obtainable by repeated convolutions of assumed spectral density functions.

Acknowledgement The author is indebted to Messrs. T. A. Barr, L. Malone, Olen Ely and their associates at the George C. Marshall Space Flight Center, National Aeronautics and Space Administration, Huntsville, Alabama, for many helpful discussions of the results of their propagation measurements in the Saturn test series. Figures I through 4 of this paper are either based on or directly adapted from References 1 and 2. Discussions with T. Kaliszewski and A. F. Ghais of ADCOM, Inc., are also gratefully acknowledged. The author is also grateful to Mr. Robert C. Barto of the White Sands Missile Range, White Sands, New Mexico, for his interest in and encouragement of this paper.

References

1. Olen Ely, R. W. Hockenberger, P. Howell and G. Boone, Radio Frequency Evaluation of SA-4, SA-5, SA-6 and SA-7, NASA Technical Memoranda, George C. Marshall Space Flight Center, Huntsville, Alabama.
2. Olen Ely and R. W. Hockenberger, Rocket exhaust effects on radio frequency transmission, Paper presented at the Sixth Solid Propellant Rocket Conference of the American Institute of Aeronautics and Astronautics, Washington, D. C. , Feb. 3, 1965.
3. W. H. Drake and F. S. Howell, Radio frequency propagation to and from ICBM's and IRBM's, Proceedings of the 1960 National Telemetry Conference.
4. D. G. Brennan, Fluctuation phenomena in space propagation, Chapter 4 of Space Communications, A. V. Balakrishnan (Ed.), McGraw-Hill Book Company, New York, 1963.
5. R. S. Lawrence, C. G. Little and H. J. A. Chivers, A survey of ionospheric effects upon earth-space radio propagation, Proc. IEEE, Vol. 52, No. 1, pp. 4-27, January, 1964.
6. H. G. Booker and W. E. Gordon, A theory of radio scattering in the troposphere, Proc. IRE, Vol. 38, No. 4, pp. 401-412, April, 1950.
7. M. P. Bachynski, I. P. French, and G. G. Cloutier, Antenna noise temperature in plasma environment, Proc. IRE, Vol. 49, No. 12, pp. 1846-1857, December, 1961.
8. M. S. Corrington, Frequency modulation distortion caused by multipath transmission, Proc. IRE, Vol. 33, No. 12, pp. 878-891, December 1945.
9. H. D. Becker, "Distortion in a Frequency Modulation System Caused by Interfering FM Signals on the Same Carrier Frequency," M. S. Thesis in the University of Buffalo Graduate School of Arts and Sciences, February, 1958.

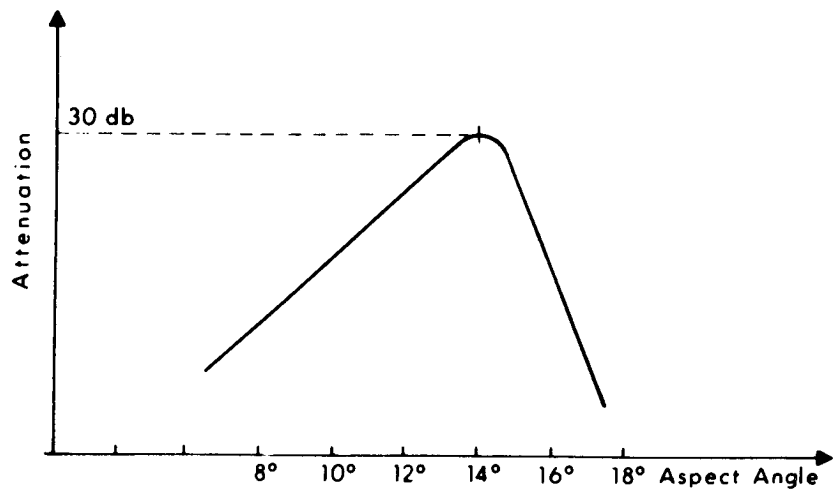
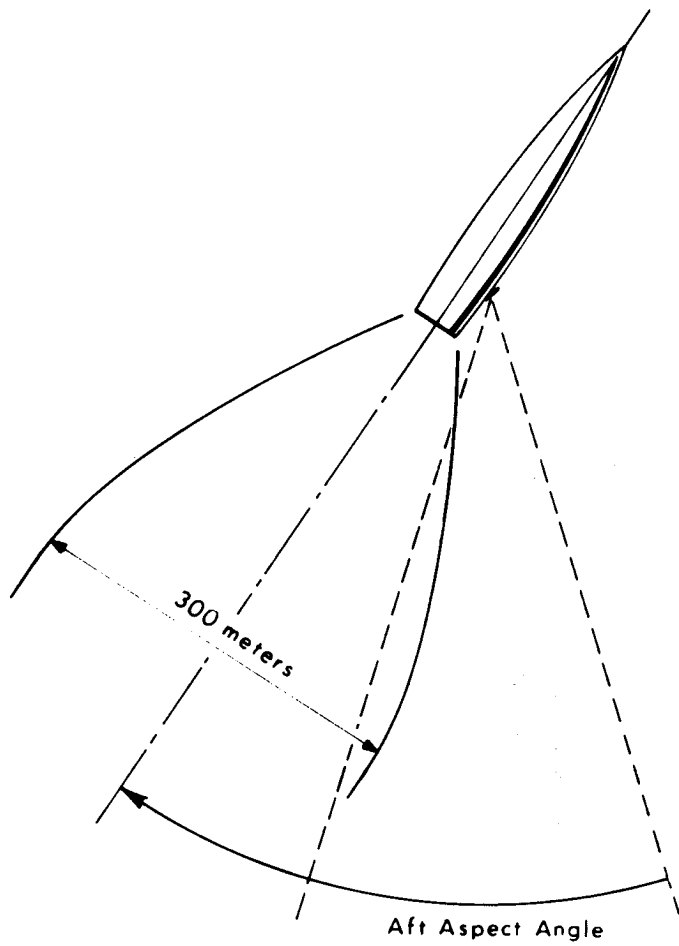


Fig. 1 -Dependence of Saturn Booster Flame Attenuation Upon Aspect Angle

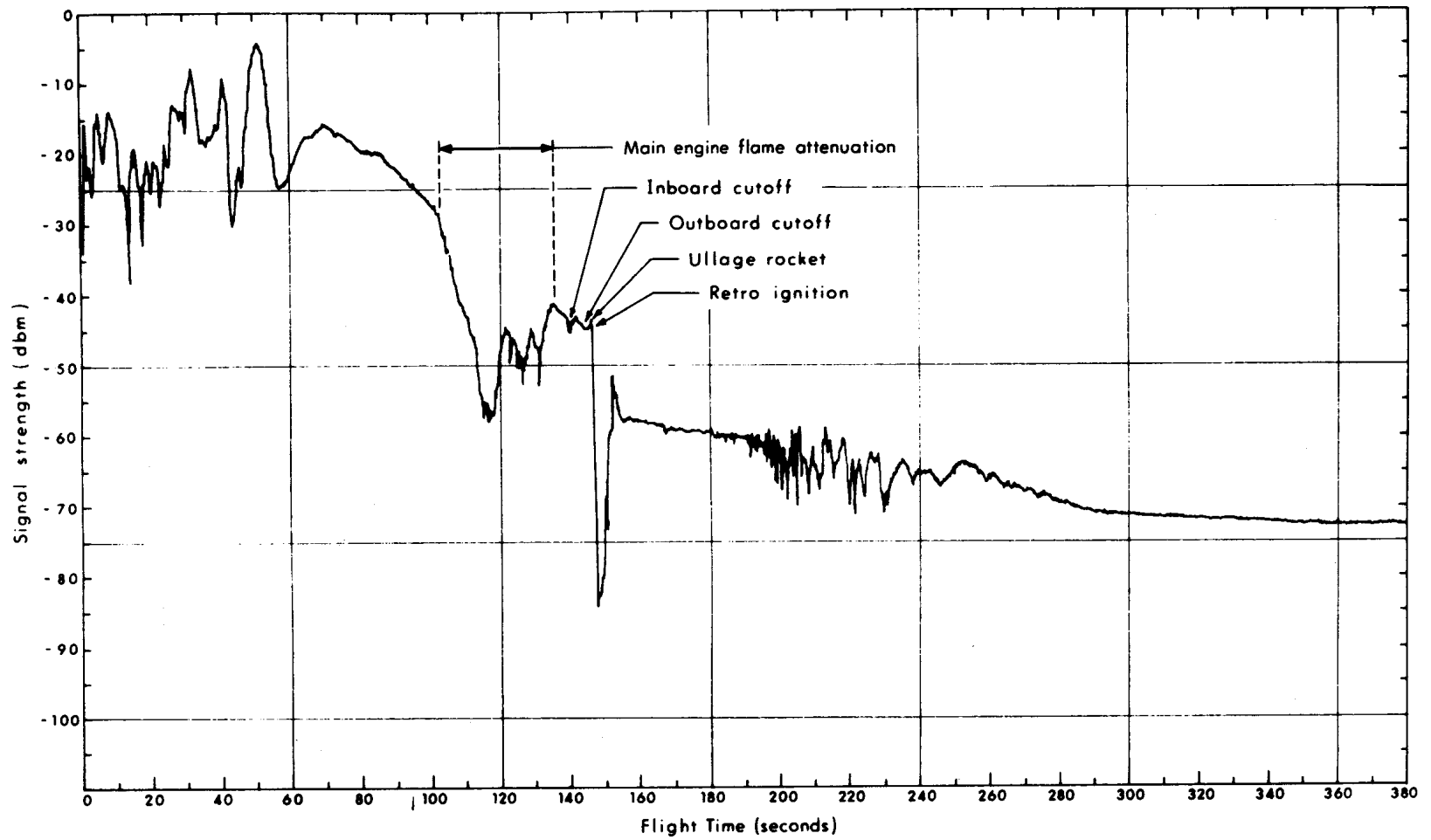


Fig. 2 -Record of Signal Envelope Fluctuations, Cape Telemetry 2, Link P1

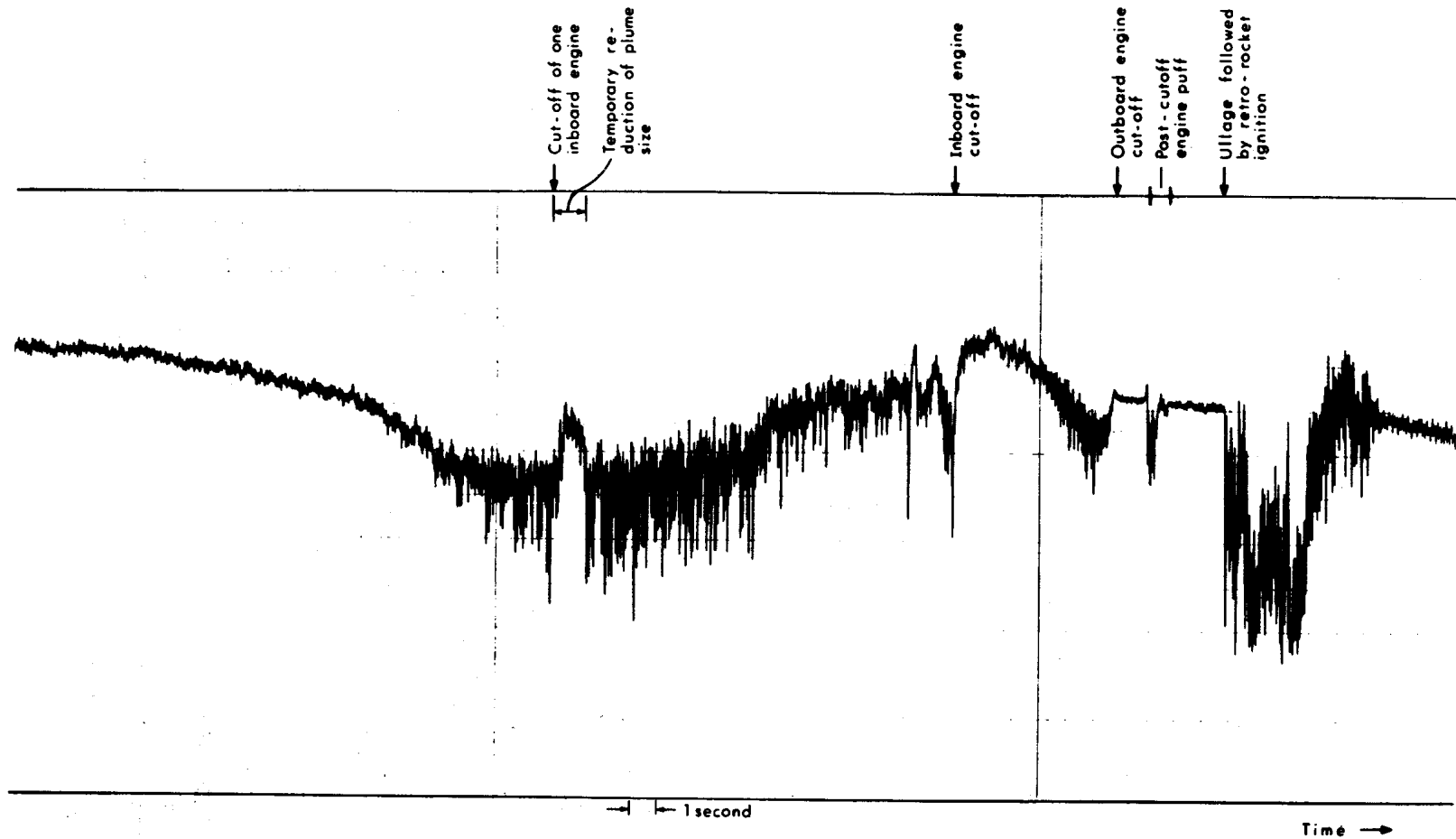


Fig. 3 -Signal Strength Recording with Expanded Time Scale (SA-4)

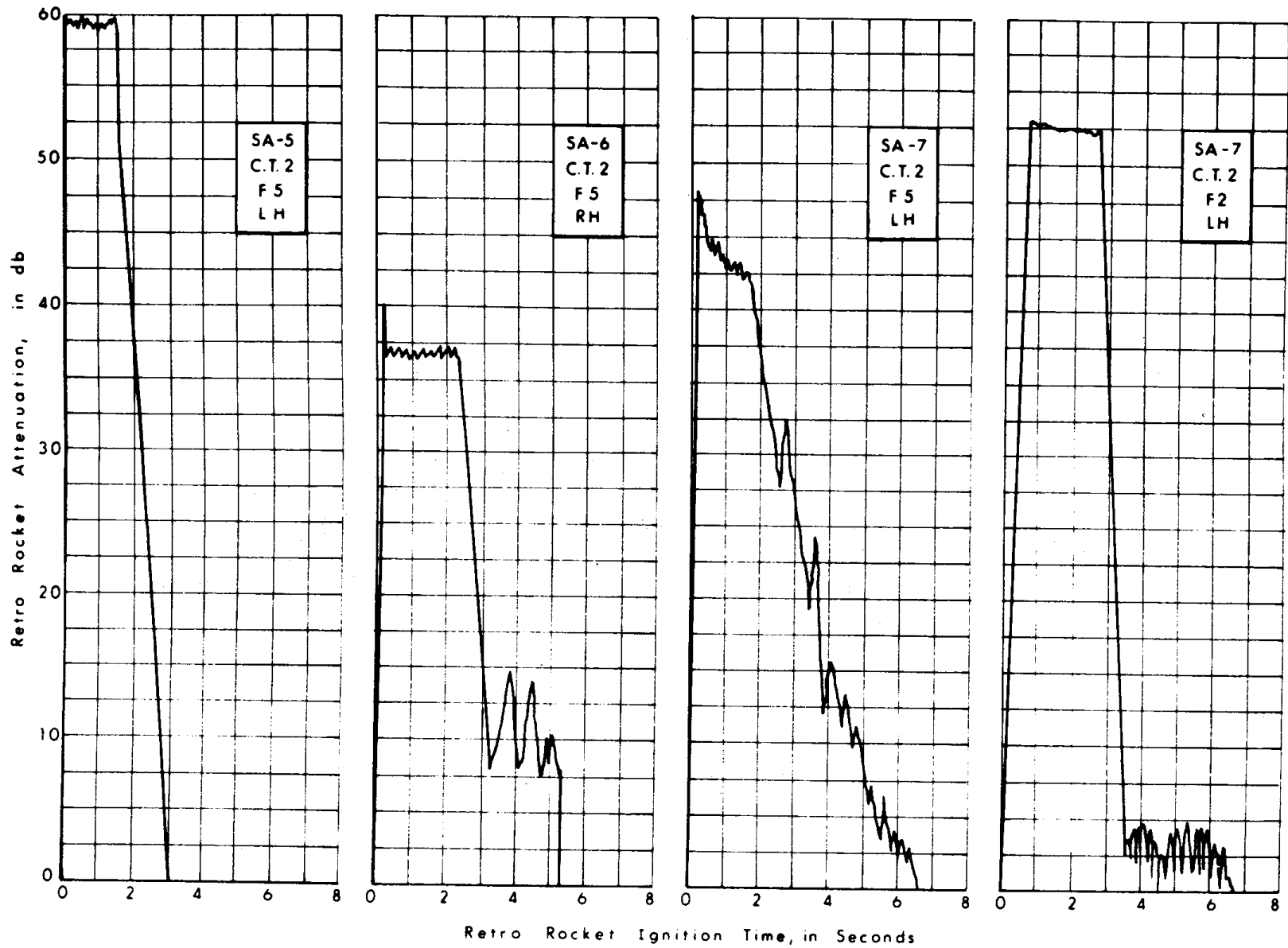


Fig. 4 - Retro-Rocket Attenuation

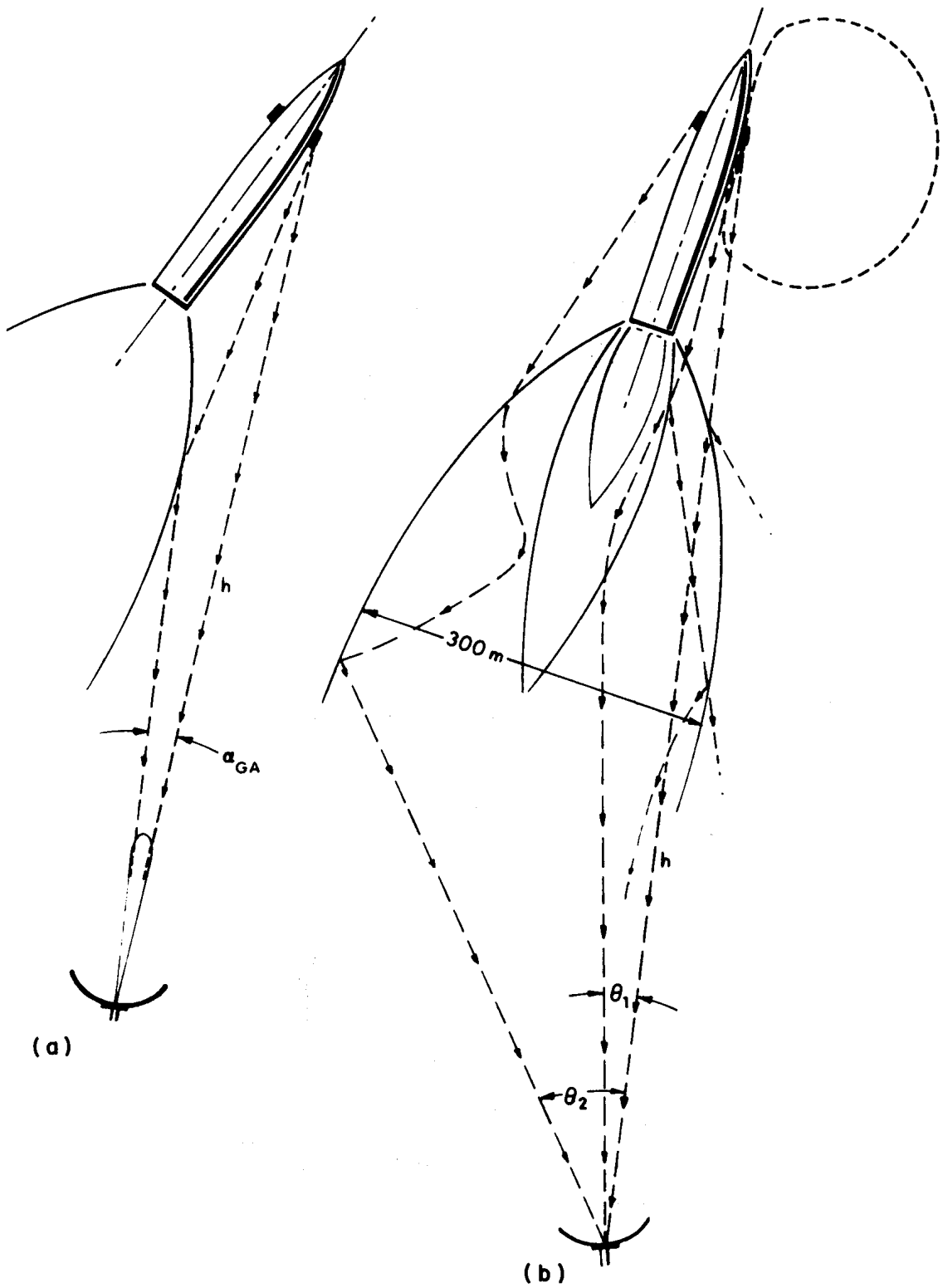


Fig. 5 -Mechanisms of Multipath Associated with Exhaust Plasma

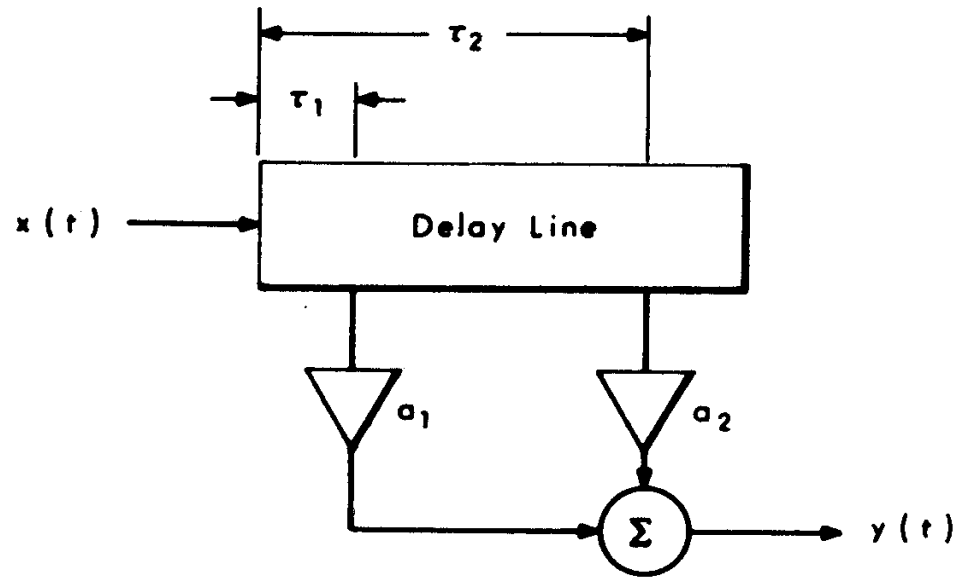


Fig. 6 -Simple Model of a Two-Path Transmission Channel

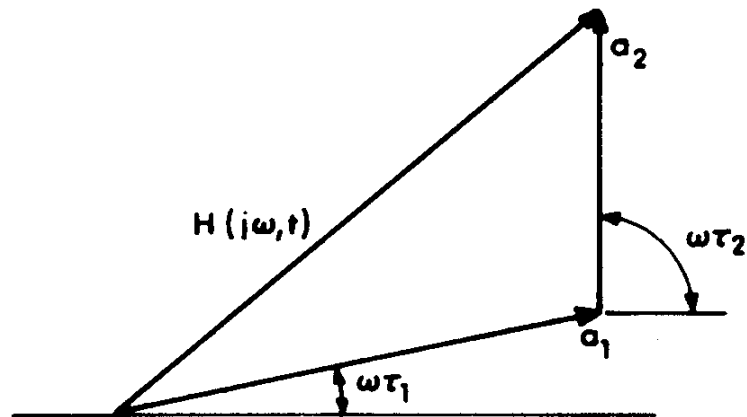


Fig. 7 -Phasor Diagram for Two-Path Line-of-Sight Propagation

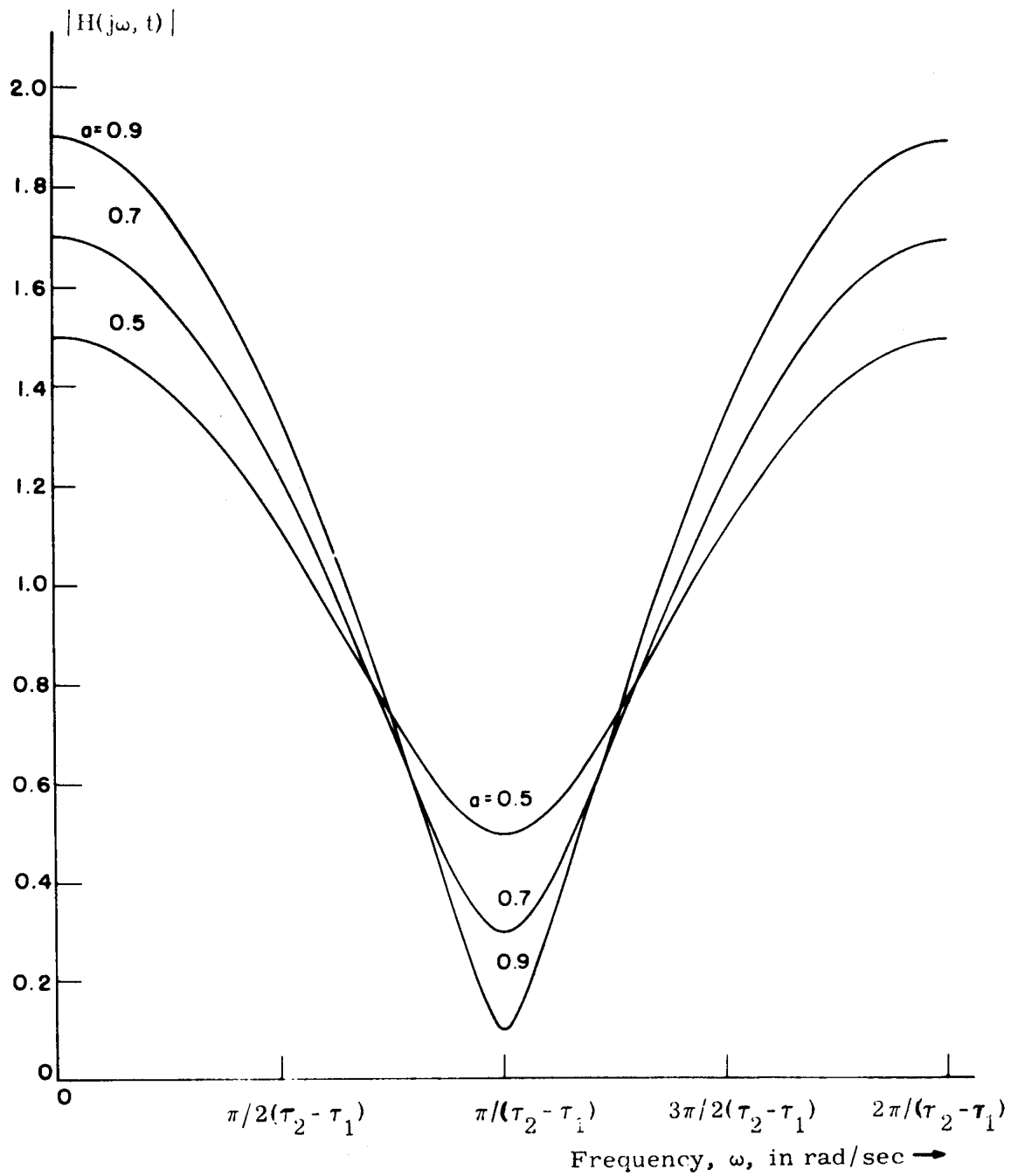


Fig. 8 Instantaneous transfer function for slowly variable two-path channels.